Applied Physics Letters

Low-frequency noise in irradiated graphene FETs

Cite as: Appl. Phys. Lett. **113**, 193502 (2018); https://doi.org/10.1063/1.5051658
Submitted: 10 August 2018 . Accepted: 22 October 2018 . Published Online: 07 November 2018

Ting Wu, Abdullah Alharbi, Takashi Taniguchi, Kenji Watanabe, and Davood Shahrjerdi

Low-frequency noise in irradiated graphene FETs

Ting Wu,[1] Abdullah Alharbi,[1] Takashi Taniguchi,[2] Kenji Watanabe,[2] and Davood Shahrjerdi[1,3,a)]
[1]*Department of Electrical and Computer Engineering, New York University, Brooklyn, New York 11201, USA*
[2]*Advanced Materials Laboratory, National Institute of Materials Science, 1-1 Namiki Tsukuba, Ibaraki 305-0044, Japan*
[3]*Center for Quantum Phenomena, Physics Department, New York University, New York, New York 10003, USA*

(Received 10 August 2018; accepted 22 October 2018; published online 7 November 2018)

We present a quantitative analysis of the low-frequency noise in irradiated monolayer graphene. In this study, we repeatedly irradiate a back-gated graphene transistor with argon ions at 90 eV and measure its low-frequency noise and channel conductivity after each irradiation. Our results indicate that the noise amplitude decreases monotonically with the increasing density of vacancy defects. The combination of our low-frequency noise measurements and carrier transport studies reveals that the mobility fluctuation model can explain this observation and that the density of vacancy defects, the density of charged impurities, and the mean free path of charge carriers determine the noise amplitude. *Published by AIP Publishing.* https://doi.org/10.1063/1.5051658

Owing to its unique properties, graphene has been explored for a variety of device applications from radio-frequency (RF) transistors[1] to biochemical sensors.[2] In almost all applications, the low-frequency noise characteristics of graphene are central to the device performance. For example, an up-conversion of the low-frequency noise in a RF transistor can contribute to the phase noise at the carrier frequency.[3] Furthermore, the amplitude of the low-frequency noise determines the detection limit of transistor-based biochemical sensors.[4] Therefore, to reduce its detrimental effect on the device performance, previous studies have extensively investigated the sources of low-frequency noise in graphene transistors.[5–19] Among those, a recent study has shown that creating defects through electron-beam (e-beam) irradiation of monolayer graphene can reduce the amplitude of the low-frequency noise and that the mobility fluctuation model can explain this observation.[15] This method of noise reduction can particularly be an attractive choice for some device applications, where the graphene mobility is not a critical factor, e.g., in biochemical sensors. Obtaining quantitative insights into this phenomenon is therefore essential for using this method in a device technology.

Here, we present a quantitative study of the low-frequency noise in irradiated graphene. To create vacancy defects, we bombarded monolayer graphene using low-energy (90 eV) argon (Ar) ions. Our device characterization results confirm that this irradiation process uniformly creates neutral defects that are short-range resonant-like scatterers in monolayer graphene. To mitigate the effect of charged-impurity Coulomb (long-range) scattering originating from an oxide substrate (e.g., SiO_2), we fabricated the graphene devices on a hexagonal boron nitride (h-BN) support substrate. To analyze the measured low-frequency noise of the irradiated graphene, we examined the carrier transport at different defect densities and then applied those findings to the mobility fluctuation model. Our analysis reveals that the density of vacancy defects, the density of charged impurities, and the mean free path of charge carriers determine the noise amplitude in our irradiated graphene.

In our experiments, we fabricated four-point back-gated field-effect transistors (FETs) from monolayer graphene, where graphene was grown on a copper foil by chemical vapor deposition (ACS material). Figure 1(a) shows the schematic of the device cross-section. The fabrication process began with the chemical removal of the copper foil, followed by the graphene transfer onto a p^+ Si substrate covered with 285 nm SiO_2. Using nanofabrication, the transferred graphene film was then patterned into small islands. In parallel, h-BN flakes were mechanically exfoliated onto another SiO_2/Si substrate. Next, we used a stamp-assisted transfer method[20] for constructing graphene-BN structures onto a fresh SiO_2/Si substrate from the samples containing individual graphene islands and h-BN flakes. After the stacking process, we performed ultrahigh vacuum annealing at 300 °C. Cr/Au (5/50 nm) metal electrodes were then formed using a combination of e-beam lithography, e-beam evaporation, and metal lift-off. Finally, the active region of the FETs was defined by e-beam lithography, followed by patterning the excess graphene in an oxygen plasma. Figure 1(b) shows the top-view optical image of a final device.

After the fabrication process, we repeatedly bombarded a candidate graphene device with low-energy Ar ions at 90 eV. Previous studies have shown that this ion energy generates mostly single vacancies in graphene[21] and that those defects add localized energy states at the Dirac point.[22] Each irradiation treatment increased the density of vacancy defects in the graphene FET. We then measured the electrical characteristics (specifically, intrinsic channel conductance and low-frequency noise characteristics) of the device in between each treatment. Through these experiments, we obtained a comprehensive set of conductivity and noise data for irradiated graphene with different defect densities. We analyzed this dataset to gain quantitative insights into the low-frequency noise characteristics of the irradiated graphene.

To quantify the defect density after each irradiation, we used Raman spectroscopy. Figure 1(c) shows the Raman

a)Electronic mail: davood@nyu.edu

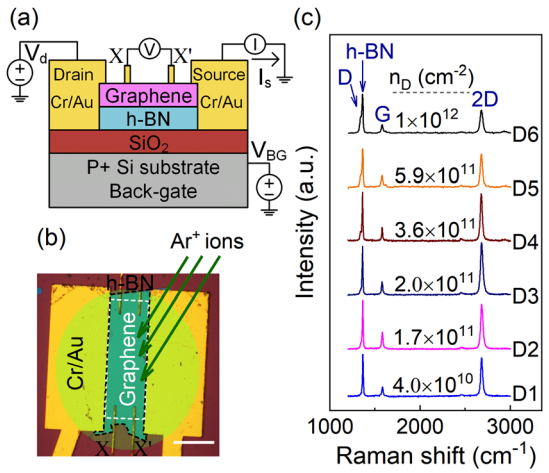

FIG. 1. (a) Schematic illustration and (b) optical image of the four-point back-gated graphene FET. The scale bar is 20 μm. In our measurements, V_{ds} was 50 mV. Defects were generated in graphene through low-energy Ar irradiation. (c) Raman spectra of the graphene channel after each irradiation step and the corresponding defect density n_D.

spectra taken from the channel region of our candidate graphene device after each irradiation. We estimated the average density of point defects (n_D) using the theoretical method by Cançado *et al.*[23] Specifically, this method estimates the average distance between point defects (L_D) from the area ratio of the D and G peaks and the line width of the G-band. In our study, we covered a wide range of point defect densities ($n_D = L_D^{-2}$) from $D1 = 4 \times 10^{10}$ to $D6 = 1 \times 10^{12}\,cm^{-2}$. Moreover, in our CVD graphene films, the density of line defects (e.g., grain boundaries) is small and falls below the measurable limit of the Raman technique. Therefore, in this study, we ignored the effect of the line defects on the transport properties of the charge carriers and on the low-frequency noise characteristics of our graphene devices.

Next, we measured the low-frequency noise characteristics of the candidate graphene FET after each irradiation. Figure 2(a) shows the normalized current noise power

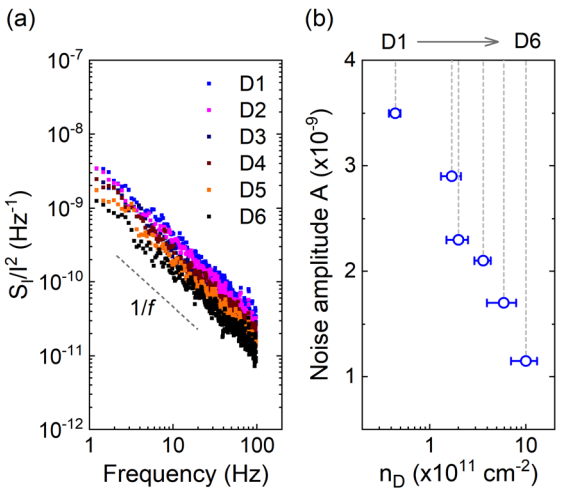

FIG. 2. (a) Normalized current noise power density of the irradiated graphene for six different defect densities, measured at $V_{BG,\,Dirac}$. (b) The noise amplitude A decreased with the increasing defect density of the irradiated graphene.

density S_I/I^2 measured at the Dirac point voltage ($V_{BG,\,Dirac}$). Consistent with a previous report by Hossain *et al.*,[15] we observed a monotonic reduction of S_I/I^2 with the increasing defect density. Furthermore, the measured noise characteristics of the device showed a 1/f dependency. We then calculated the noise amplitude (A) from the measured spectral noise density of the irradiated graphene at different defect densities using[15,17]

$$A = \frac{1}{M}\sum_{j=1}^{M} f_j \times \left(\frac{S_I}{I^2}\right)_j, \tag{1}$$

where $(S_I/I^2)_j$ is the normalized noise power density measured at the frequency f_j and $1 \le f_j \le 100$ Hz. From the noise measurements, we found that the noise amplitude of the graphene FET gradually reduces after each irradiation, as shown in Fig. 2(b). Previous research suggests that the mobility fluctuation model of the low-frequency noise can explain this phenomenon.[15] Therefore, we used the mobility fluctuation model, discussed next, to analyze the observed reduction of the noise amplitude.

In our noise analysis, we assumed that the mobility fluctuation in the channel of the irradiated graphene FET is the only major source of the measured 1/f noise. Therefore, we neglected the contribution from the other possible sources of noise (e.g., contact resistance). We show the validity of this assumption later in this study. Accounting for the two-dimensional structure of graphene in the mobility fluctuation model,[24] we can write the following expression for the normalized spectral noise density of an elemental fluctuation event with a characteristic time of τ

$$\frac{S_I}{I^2}(f) = \frac{4N_{t\mu}}{W \cdot L}\frac{\tau\psi(1-\psi)}{1+(2\pi f\tau)^2} l_0^2(\sigma_2 - \sigma_1)^2, \tag{2}$$

where $N_{t\mu}$ is the density of a given scattering center per unit area that causes the change in the capture radius σ, ψ is the probability of the scattering center to be in a state with a capture radius of σ_1, $W \cdot L$ represents the channel area of the FET, and l_0 is the mean free path of the charge carriers in graphene. From Eq. (2), each fluctuation event is described by a Lorentzian. The superposition of these elemental events with different time constants yields the 1/f noise due to the mobility fluctuation. To gain quantitative insights into the noise amplitude, next we examined the transport properties of our irradiated graphene.

To analyze the carrier transport in the irradiated graphene, we used a combination of four-point measurements and modeling of the intrinsic channel conductivity. From this exercise, we aimed to find two important details about the transport properties of the carriers. The first one is to determine the type of the dominant scattering center in the irradiated graphene device. Having identified the type of those scattering centers, the second goal is to estimate the mean free path of the carriers. In Fig. 3(a), the solid curves are the measured intrinsic channel conductivity [$G^{-1} = (W/L) \cdot (V_X - V_{X'})/I_s$, see Fig. 1(a)] of the graphene FET after each irradiation step. Two key observations can be made from the conductivity plot. First, the minimum conductivity, which occurs at the Dirac point voltage,

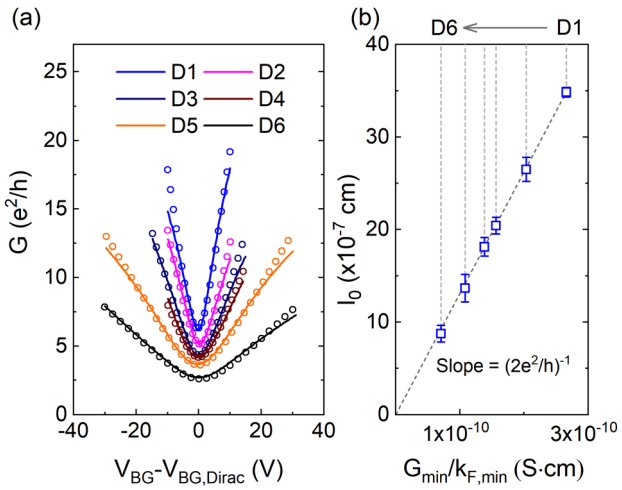

FIG. 3. (a) Intrinsic conductivity of the irradiated graphene device for six different defect densities. Solid lines represent the measured data. The symbols are the fits to the experimental data using Eq. (5). (b) Mean free path of carriers decreased with the increasing defect density.

decreased with increasing defect density. Second, the conductivity curves became consistently broader after each irradiation step. These observations agree with the previous reports on the conductivity of the irradiated graphene FETs.[25]

Charged impurities cause long-range carrier scattering in graphene, resulting in a conductivity[26]

$$G_C = \frac{2e^2}{h}\frac{n_{\text{tot}}}{n_{\text{C}}}\frac{1}{\Gamma(2r_s)}, \tag{3}$$

where n_{tot} and n_{C} are the total density of charge carriers at each gate voltage (V_{BG}) and the density of charged impurities. Furthermore, e, h, r_s, and $\Gamma(2r_s)$ are the elementary charge, the Planck constant, the Wigner-Seitz radius, and the analytical function of dimensionless interaction strength in graphene. Moreover, previous studies have shown that charged impurities also create electron-hole puddles in graphene, resulting in residual charges with a density of n_{min}.[26,27] In our analysis of the graphene conductivity, we calculated r_s, $\Gamma(2r_s)$, and $n_{\text{min}}/n_{\text{C}}$ using the theoretical equations by Adam *et al.*[26]

In the case of the irradiated graphene, one must also account for the effect of vacancy defects on the conductivity. Previous theoretical studies have predicted that vacancies in monolayer graphene yield scattering centers that have resonant-like characteristics.[28] By modeling each vacancy defect as a potential well of radius R, the conductivity of graphene due to these defects can be obtained from[29,30]

$$G_D = \frac{2e^2}{\pi h}\frac{n_{\text{tot}}}{n_{\text{D}}}\ln^2(k_F R), \tag{4}$$

where n_{D} is the defect density, $k_F\left(=\sqrt{\pi n_{\text{tot}}}\right)$ is the Fermi wave vector, and R is the range of the scattering center. To apply this resonant impurity model, defects must satisfy two requirements. First, defects must be neutral, that is, they should not break the electron-hole charge symmetry. Consequently, n_{min} remains unchanged with the increasing defect density. Second, the resulting scattering centers must have a range much shorter than the Fermi wavelength and possibly on the order of the graphene lattice constant a, i.e., $a \lesssim R \ll 1/k_F$.

To consider the effects of both charged impurities and vacancy defects on the graphene conductivity, we used the Matthiessen rule

$$G = (G_C^{-1} + G_D^{-1})^{-1} = \frac{2e^2}{h} n_{\text{tot}}\left(\frac{\pi n_{\text{D}}}{\ln^2(k_F R)} + n_{\text{C}}\Gamma(2r_s)\right)^{-1}. \tag{5}$$

We then used the above equation to fit the measured channel conductivity curves in Fig. 3(a). To do so, we used R and n_{C} as the fitting parameters and replaced n_D with the density of defects estimated from the Raman measurements. Furthermore, we evaluated n_{tot} using

$$n_{\text{tot}} = \sqrt{(n_{\text{min}}^2 + n[V_{\text{BG}}^*])^2}, \tag{6}$$

where $n[V_{\text{BG}}^*]$ was obtained from[31]

$$V_{\text{BG}}^* = V_{\text{BG}} - V_{\text{BG,Dirac}} = \frac{e}{C_{\text{ox}}}n + \frac{\hbar v_F\sqrt{\pi n}}{e}. \tag{7}$$

In this equation, n, C_{ox}, and v_F represent the charge carrier density induced by the back-gate bias, the oxide capacitance, and the Fermi velocity. In our calculations, we used $C_{\text{ox}} = 1.2 \times 10^{-8}\,\mu\text{F/cm}^2$ and $v_F = 1.1 \times 10^8$ cm/s. We obtained reasonable fits to the measured conductivity data using Eq. (5), the symbols in Fig. 3(a).

Table I shows the summary of the curve fitting results for the different irradiation conditions. From the data, it is evident that while n_{D} of the graphene FET was varied by almost 25 times, n_{min} changed only by about a factor of 3, indicating that the defects generated by the irradiation process are neutral. In particular, n_{min} remained nearly unchanged for the irradiation conditions of D1–D4, but the gradual increase in n_{min} beyond D4 is noticeable. We speculate that beyond this irradiation condition, the Ar bombardment began to damage the underlying h-BN substrate, creating additional charged impurities. Furthermore, we found that all the measured conductivity curves can only be fitted using a scattering range (R) of 0.9–1.2 Å, which satisfies the requirement of the resonant impurity model, i.e., $a \lesssim R \ll 1/k_F$. These two observations validate our use of Eq. (4) for estimating the graphene conductivity due to the defects generated by the irradiation process.

Having established that the carrier transport in our irradiated graphene device, at least at low carrier densities, is

TABLE I. Summary of n_{D}, n_{C}, and n_{min} for different irradiation conditions.

Condition	n_{D} (cm^{-2})	n_{C} (cm^{-2})	n_{min} (cm^{-2})
D1	0.4×10^{11}	0.9×10^{12}	2.3×10^{11}
D2	1.7×10^{11}	1.1×10^{12}	2.6×10^{11}
D3	2.0×10^{11}	1.6×10^{12}	3.4×10^{11}
D4	3.6×10^{11}	1.7×10^{12}	3.5×10^{11}
D5	5.9×10^{11}	2.5×10^{12}	4.5×10^{11}
D6	10×10^{11}	4.4×10^{12}	7.1×10^{11}

primarily dominated by the neutral defects and the charged impurities, we can obtain an expression for the mean free path at the Dirac point (where $n_{tot} = n_{min}$). To do so, we used Eq. (5) together with the diffusive conductivity model of graphene, resulting in

$$l_0 = \sqrt{\frac{n_{\min}}{\pi}}\left(\frac{\pi n_D}{\ln^2(k_{F,min}R)} + n_C\Gamma(2r_s)\right)^{-1}. \quad (8)$$

Figure 3(b) shows the calculated mean free path for the irradiation conditions D1–D6. In this plot, G_{min} is the measured conductivity at the Dirac point and $k_{F,min} = \sqrt{\pi n_{min}}$ was calculated using the corresponding n_{min} data in Table I. As expected, the mean free path decreased monotonically with the increasing defect density in graphene.

Next, we revisited the noise amplitude data in light of the above analysis of the carrier transport in the irradiated graphene. Assuming that the mobility fluctuation is the dominant source of noise in our irradiated graphene, we can simply use Eq. (8) to substitute l_0 in Eq. (2). However, less understood for further analysis of the graphene noise using the mobility fluctuation model is the quantification of the density of scattering centers that contribute to the mobility fluctuation [i.e., $N_{t\mu}$ in Eq. (2)]. Interestingly, we found that the plot of the noise amplitude data for D1–D6 as a function of $(n_C + n_D)l_0^2$, as shown in Fig. 4(a), follows a linear trend. This observation suggests that the mobility fluctuation model can explain the noise amplitude of our irradiated graphene and that $N_{t\mu}$ in our irradiated graphene is proportional to the total density of charged impurities and vacancy defects. The apparent linear trend of the noise data in Fig. 4(a) also suggests that although the carrier scattering mechanisms by the charged impurities and the vacancy defects are different from one another, their effects on the mobility fluctuation in the measured frequency band are similar. Although we currently do not understand the underlying physics of the linear trend in our data, our observation may provide a basis for future investigations into the origin of this phenomenon.

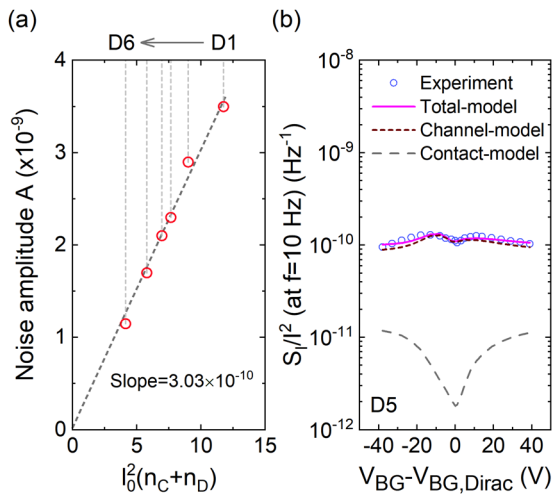

FIG. 4. (a) The apparent linear trend of the noise data suggests that (1) the mobility fluctuation model can explain the low-frequency noise characteristics of our irradiated graphene; (2) N_{tu} is proportional to $n_C + n_D$; and (3) the effects of charged impurities and vacancy defects on mobility fluctuation are similar. (b) Contribution of contact resistance fluctuation to the total noise in our graphene FET is negligible.

Finally, we comment on the contribution of the metal contact resistance to the overall low-frequency noise in our graphene device and show that it is negligible. The normalized noise power density due to the contributions of the graphene channel and the contacts is given by[32]

$$\frac{S_I}{I^2} = \frac{S_{RCH}}{R_{CH}^2}\frac{R_{CH}^2}{R_{tot}^2} + \frac{S_{RC}}{R_C^2}\frac{R_C^2}{R_{tot}^2}, \quad (9)$$

where S_{RCH}/R_{CH}^2 and S_{RC}/R_C^2 are the noise spectral density of the channel resistance and the contact resistance fluctuations, respectively. Furthermore, R_{CH}, R_C, and R_{tot} denote the resistance of the graphene channel, the contact resistance, and the total resistance (i.e., $R_{CH} + R_C$). In our analysis, we determined these resistances from the four-point measurements. From those measurements, we found that the contribution of R_C to the total resistance in all cases was less than 15%. Figure 4(b) shows the summary of our analysis for the irradiation condition D_5. This condition represents the worst-case scenario since $R_C/R_{tot} = 0.15$. To fit the experimental data, we found S_{RCH}/R_{CH}^2 and S_{RC}/R_C^2 at each back-gate voltage based on a minimum mean-square error estimation. The results in Fig. 4(b) confirm the validity of our earlier assumption, where we ignored the contribution of the contact noise for analyzing the noise amplitude of our irradiated graphene FET.

In conclusion, our study indicates that the mobility fluctuation model of the low-frequency noise can explain the reduction of the noise amplitude in our irradiated graphene. We find that the density of the scattering centers that are responsible for mobility fluctuation appears to be proportional to the total density of charge impurities and vacancy defects. The findings of our study may be used as a basis for developing a predictive noise model that allows the precise engineering of the low-frequency noise of graphene FETs through irradiation.

This work was supported by the NSF (Grant Nos. CMMI-1728051 and MRI-1531664) and the Gordon and Betty Moore Foundation (Grant No. GBMF 4838). This research used resources of the Center for Functional Nanomaterials, which is a U.S. DOE Office of Science Facility, at Brookhaven National Laboratory under Contract No. DE-SC0012704. We acknowledge the Surface Science Facility of CUNY Advanced Science Research Center.

[1]L. Liao, Y.-C. Lin, M. Bao, R. Cheng, J. Bai, Y. Liu, Y. Qu, K. L. Wang, Y. Huang, and X. Duan, "High-speed graphene transistors with a self-aligned nanowire gate," Nature **467**, 305 (2010).
[2]W. Fu, L. Jiang, E. P. van Geest, L. M. Lima, and G. F. Schneider, "Sensing at the surface of graphene field-effect transistors," Adv. Mater. **29**, 1603610 (2017).
[3]A. A. Balandin, *Noise and Fluctuations Control in Electronic Devices* (American Scientific Publishers, Stevenson Ranch, CA, 2002).
[4]T. Wu, A. Alharbi, K.-D. You, K. Kisslinger, E. A. Stach, and D. Shahrjerdi, "Experimental study of the detection limit in dual-gate biosensors using ultrathin silicon transistors," ACS Nano **11**, 7142–7147 (2017).
[5]Z. Chen, Y.-M. Lin, M. J. Rooks, and P. Avouris, "Graphene nano-ribbon electronics," Physica E **40**, 228–232 (2007).
[6]Y.-M. Lin and P. Avouris, "Strong suppression of electrical noise in bilayer graphene nanodevices," Nano Lett. **8**, 2119–2125 (2008).

[7]Q. Shao, G. Liu, D. Teweldebrhan, A. A. Balandin, S. Rumyantsev, M. S. Shur, and D. Yan, "Flicker noise in bilayer graphene transistors," IEEE Electron Device Lett. **30**, 288–290 (2009).
[8]G. Liu, W. Stillman, S. Rumyantsev, Q. Shao, M. Shur, and A. Balandin, "Low-frequency electronic noise in the double-gate single-layer graphene transistors," Appl. Phys. Lett. **95**, 033103 (2009).
[9]A. N. Pal and A. Ghosh, "Ultralow noise field-effect transistor from multilayer graphene," Appl. Phys. Lett. **95**, 082105 (2009).
[10]S. Rumyantsev, G. Liu, W. Stillman, M. Shur, and A. Balandin, "Electrical and noise characteristics of graphene field-effect transistors: Ambient effects, noise sources and physical mechanisms," J. Phys.: Condens. Matter **22**, 395302 (2010).
[11]Y. Zhang, E. E. Mendez, and X. Du, "Mobility-dependent low-frequency noise in graphene field-effect transistors," ACS Nano **5**, 8124–8130 (2011).
[12]G. Liu, S. Rumyantsev, M. Shur, and A. A. Balandin, "Graphene thickness-graded transistors with reduced electronic noise," Appl. Phys. Lett. **100**, 033103 (2012).
[13]G. Liu, S. Rumyantsev, M. S. Shur, and A. A. Balandin, "Origin of 1/f noise in graphene multilayers: Surface vs. volume," Appl. Phys. Lett. **102**, 093111 (2013).
[14]S. Rumyantsev, D. Coquillat, R. Ribeiro, M. Goiran, W. Knap, M. Shur, A. Balandin, and M. Levinshtein, "The effect of a transverse magnetic field on 1/f noise in graphene," Appl. Phys. Lett. **103**, 173114 (2013).
[15]M. Zahid Hossain, S. Rumyantsev, M. S. Shur, and A. A. Balandin, "Reduction of 1/f noise in graphene after electron-beam irradiation," Appl. Phys. Lett. **102**, 153512 (2013).
[16]A. A. Balandin, "Low-frequency 1/f noise in graphene devices," Nat. Nanotechnol. **8**, 549 (2013).
[17]M. A. Stolyarov, G. Liu, S. L. Rumyantsev, M. Shur, and A. A. Balandin, "Suppression of 1/f noise in near-ballistic h-BN-graphene-h-BN heterostructure field-effect transistors," Appl. Phys. Lett. **107**, 023106 (2015).
[18]M. Kumar, A. Laitinen, D. Cox, and P. J. Hakonen, "Ultra low 1/f noise in suspended bilayer graphene," Appl. Phys. Lett. **106**, 263505 (2015).
[19]H. N. Arnold, V. K. Sangwan, S. W. Schmucker, C. D. Cress, K. A. Luck, A. L. Friedman, J. T. Robinson, T. J. Marks, and M. C. Hersam, "Reducing flicker noise in chemical vapor deposition graphene field-effect transistors," Appl. Phys. Lett. **108**, 073108 (2016).
[20]A. Castellanos-Gomez, M. Buscema, R. Molenaar, V. Singh, L. Janssen, H. S. Van Der Zant, and G. A. Steele, "Deterministic transfer of two-dimensional materials by all-dry viscoelastic stamping," 2D Mater. **1**, 011002 (2014).
[21]O. Lehtinen, J. Kotakoski, A. Krasheninnikov, A. Tolvanen, K. Nordlund, and J. Keinonen, "Effects of ion bombardment on a two-dimensional target: Atomistic simulations of graphene irradiation," Phys. Rev. B **81**, 153401 (2010).
[22]M. M. Ugeda, I. Brihuega, F. Guinea, and J. M. Gómez-Rodríguez, "Missing atom as a source of carbon magnetism," Phys. Rev. Lett. **104**, 096804 (2010).
[23]L. G. Cançado, M. G. da Silva, E. H. M. Ferreira, F. Hof, K. Kampioti, K. Huang, A. Pénicaud, C. A. Achete, R. B. Capaz, and A. Jorio, "Disentangling contributions of point and line defects in the Raman spectra of graphene-related materials," 2D Mater. **4**, 025039 (2017).
[24]A. Dmitriev, M. Levinshtein, and S. Rumyantsev, "On the Hooge relation in semiconductors and metals," J. Appl. Phys. **106**, 024514 (2009).
[25]J.-H. Chen, W. Cullen, C. Jang, M. Fuhrer, and E. Williams, "Defect scattering in graphene," Phys. Rev. Lett. **102**, 236805 (2009).
[26]S. Adam, E. Hwang, V. Galitski, and S. D. Sarma, "A self-consistent theory for graphene transport," Proc. Natl. Acad. Sci. **104**, 18392–18397 (2007).
[27]J. Martin, N. Akerman, G. Ulbricht, T. Lohmann, J. V. Smet, K. Von Klitzing, and A. Yacoby, "Observation of electron–hole puddles in graphene using a scanning single-electron transistor," Nat. Phys. **4**, 144 (2008).
[28]M. Katsnelson and K. Novoselov, "Graphene: New bridge between condensed matter physics and quantum electrodynamics," Solid State Commun. **143**, 3–13 (2007).
[29]T. Stauber, N. Peres, and F. Guinea, "Electronic transport in graphene: A semiclassical approach including midgap states," Phys. Rev. B **76**, 205423 (2007).
[30]M. Monteverde, C. Ojeda-Aristizabal, R. Weil, K. Bennaceur, M. Ferrier, S. Guéron, C. Glattli, H. Bouchiat, J. Fuchs, and D. Maslov, "Transport and elastic scattering times as probes of the nature of impurity scattering in single-layer and bilayer graphene," Phys. Rev. Lett. **104**, 126801 (2010).
[31]S. Kim, J. Nah, I. Jo, D. Shahrjerdi, L. Colombo, Z. Yao, E. Tutuc, and S. K. Banerjee, "Realization of a high mobility dual-gated graphene field-effect transistor with Al_2O_3 dielectric," Appl. Phys. Lett. **94**, 062107 (2009).
[32]J. Renteria, R. Samnakay, S. Rumyantsev, C. Jiang, P. Goli, M. Shur, and A. Balandin, "Low-frequency 1/f noise in MoS_2 transistors: Relative contributions of the channel and contacts," Appl. Phys. Lett. **104**, 153104 (2014).